mathematics

MDPI

Article

Multi-Condition Rolling Bearing Fault Denoising Method and Application Based on RIME-VMD

Xin Zhao [1], Xuebin Liu [1,2] and Hanshan Li [2,*]

[1] School of Information Engineering, Shanghai Zhongqiao Vocational and Technical University, Shanghai 201514, China; zhaoxin@shzq.edu.cn (X.Z.); liuxuebin@st.xatu.edu.cn (X.L.)
[2] School of Electronic and Information Engineering, Xi'an Technological University, Xi'an 710021, China
* Correspondence: lihanshan269@163.com

Abstract: To improve the stability of rolling bearing fault signal denoising under different working conditions, this study proposes a multi-condition rolling bearing fault denoising method based on RIME-VMD. According to the characteristics of rolling bearing fault signal, RIME (frost and ice algorithm) is utilized to obtain adaptive optimization of the modal number and penalty factors in VMD (variational mode decomposition) algorithm, and then the optimized core parameters are input into VMD to decompose the rolling bearing fault signal. The fitness function is established by introducing the fusion of power spectrum entropy and kurtosis value; these intrinsic modal functions (IMFs) with high correlation based on original rolling bearing fault signal are selected to reconstruct the rolling bearing fault denoising signal. The experimental results show that the RIME-VMD method can effectively remove most of the noise in the rolling bearing fault signal, and the performance evaluation indexes of this method are better than other existing optimization algorithms. The research achievement of this study can provide effective data support for the fault diagnosis of bearing equipment.

Keywords: rolling bearing fault signal; denoising; variational mode decomposition (VMD); frost and ice algorithm (RIME); multiple conditions

MSC: 37M10

check for updates

Academic Editor: Jonathan Blackledge

Received: 9 March 2025
Revised: 18 April 2025
Accepted: 19 April 2025
Published: 20 April 2025

Citation: Zhao, X.; Liu, X.; Li, H. Multi-Condition Rolling Bearing Fault Denoising Method and Application Based on RIME-VMD. *Mathematics* **2025**, *13*, 1348. https://doi.org/10.3390/math13081348

Copyright: © 2025 by the authors. Licensee MDPI, Basel, Switzerland. This article is an open access article distributed under the terms and conditions of the Creative Commons Attribution (CC BY) license (https://creativecommons.org/licenses/by/4.0/).

1. Introduction

Rolling bearing is one of the important parts of mechanical equipment and is also one of the most vulnerable parts. The working state of rolling bearing determines the effective operation of the equipment [1,2]. When defects occur in the bearing outer ring, inner ring and rolling element, the vibration status signal will change [3–5]; meanwhile, this result causes the rolling bearing fault signal to have nonlinear and non-stationary characteristics. Due to the complex operating conditions of rotating machinery and equipment and serious background noise pollution, the rolling bearing fault signal is often submerged in noise, and it is difficult to find the change in the bearing wear state from the time domain waveform change in status signal [6–9]. Therefore, the noise reduction in rolling bearing fault signals to obtain effective fault characteristics is of great significance for subsequent fault signal analysis and fault diagnosis [10,11].

In the process of rolling bearing fault signal acquisition, there often exists environment noise, which influences the accuracy of fault diagnosis and means the rolling bearing fault characteristics cannot be accurately identified [12]. At present, the commonly used

methods for denoising rolling bearing fault signal include EMD (empirical mode decomposition) [13–15], CEEMD (complementary ensemble empirical mode decomposition) [16,17] and VMD (variational mode decomposition) [18,19]. However, EMD has the problems of mode aliasing and end effects. Although EEMD can effectively suppress mode aliasing through multiple EMD and superimposed Gaussian white noise, it still has problems of large reconstruction error and poor decomposition completeness. CEEMD can effectively solve these problems by adding positive and negative pairs of auxiliary white noise [20]. Zhao et al. [21] proposed a method based on the adaptive modification of CEEMD combined with a one-dimensional convolutional neural network for fault diagnosis. Both experiments verified that the classification accuracy of this method was higher than other methods. However, CEEMD has the problem that the final average results are difficult to align. VMD transforms the above problem into a variational problem to effectively solve the shortcomings of the above method. VMD is a new non-recursive signal decomposition method, which overcomes the shortcomings of the EMD algorithm such as mode aliasing and frequency effects by presetting the number of modes and central frequency. In addition, compared with CEEMD, the computational cost is greatly reduced, and it is more suitable for long sequence signals or scenes with high real-time requirements. Li et al. [22] proposed a VMD optimization method based on the principle of maximum envelope kurtosis. The finally selected IMF was analyzed through the envelope power spectrum to verify the feasibility and superiority of the optimization method. Cui et al. [23] combined VMD and maximum correlation kurtotic deconvolution for the fault diagnosis of rolling bearing elements, and through experimental verification, this method can obtain better fault accuracy. However, VMD needs to set two parameters, the number of decomposition layers and the penalty factor, according to experience before decomposition. If the parameters are set artificially, there will be certain subjectivity and poor generality [24,25]. When using the VMD algorithm to denoise a rolling bearing fault signal, it is necessary to set the modal number and quadratic penalty factor parameters in advance and use the meta heuristic algorithm to optimize the parameters. Chen et al. [26] proposed the SSA (sparrow search algorithm) to optimize SVM (support vector machine) parameters and extract rolling bearing fault characteristic parameters from multiple angles to achieve a noise reduction in the rolling bearing signal. Zhong et al. [27] determined the optimal parameters of total variational noise reduction via the PSO (particle swarm optimization) algorithm and then used the optimized total variational noise reduction algorithm to reduce the rolling bearing fault signal. Chen et al. [28] used the HHO (Harris hawk optimization) algorithm to optimize the modal component number and quadratic penalty coefficient of VMD, realized the adaptive decomposition of noise reduction signals and extracted the optimal modal component. Qin et al. [29] proposed the fault diagnosis of a transverse damper for high-speed trains based on RIME-VMD. The RIME-VMD method utilizes the efficient search and development capabilities of the RIME, which can more quickly find the globally optimal combinations of the number of decomposition layers and the penalty factor parameters in VMD for high-speed trains under different working conditions. These optimization algorithms can search for optimization parameters. Therefore, how to improve the selection of these two key parameters is crucial to the subsequent noise reduction results of multi-condition rolling bearing fault signals.

In summary, to improve the denoising effect of a rolling bearing fault signal under different working conditions, the RIME algorithm with the best filtering effect and the improved VMD algorithm are selected for signal denoising, forming the multi-condition rolling bearing fault denoising method based on RIME-VMD. The main work and contributions of this study are as follows:

(1) Taking the multi-condition rolling bearing signal as the research object, a method for rolling bearing signal decomposition based on VMD is proposed. The signal decomposition problem is constructed as a variational problem to optimize the central frequency of each modal function, so as to achieve the purpose of signal decomposition and realize the separation of effective components and noise in the signal.

(2) The RIME algorithm is used to optimize VMD parameters, and power spectrum entropy and the kurtosis value are introduced to establish a fitness function in order to obtain the best combination of VMD parameters, so as to realize the noise reduction in a multi-working condition rolling bearing fault signal and effectively retain the fault signal.

The structure of this study is as follows: The second part introduces the noise analysis of the rolling bearing signal, the third part gives the basic theory, the fourth part focuses on the multi-condition rolling bearing fault denoising method based on RIME-VMD, the fifth part is the experimental section and analysis, and, finally, the sixth part summarizes the main conclusions drawn from this study.

2. The Noise Analysis of Rolling Bearing Signal

When the rolling bearing is running, the signal received by the sensor contains both effective information about the running state of the rolling bearing and useless noise information. Among them, the noise component can be roughly divided into two parts: the inherent noise from the running of the bearing system and the random noise caused by the external environment in the actual engineering measurement. Figure 1 shows the collected rolling bearing signal. The red area represents the rolling bearing signal at a certain moment, the blue area represents the noise signal.

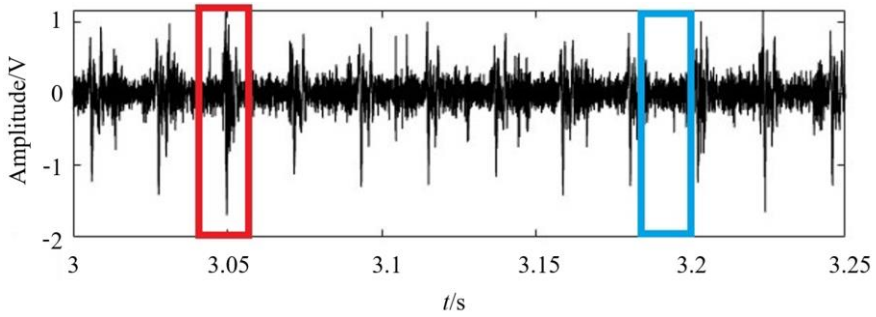


Figure 1. Rolling bearing signal.

From the result in Figure 1, we can find that there are signals in the middle- and high-frequency band in the red box area. These signals not only contain rolling bearing fault signals but also contain some bearing inherent noise, which mainly comes from the collision friction between the contact surfaces of the bearing components, such as the collision sound between the rolling body and the cage when the bearing is running at high speed and the non-Gaussian noise caused by the contact friction sound when the lubrication condition is not good. In bearing health monitoring, the rolling bearing signal collected from the high-speed running process has a high amplitude, which easily covers the fault impact characteristics of the rolling bearing and will seriously affect the detection and diagnosis of the bearing. In addition, there are low-frequency signals in the blue box area, which are mainly caused by environmental noise, and environmental noise is mainly composed of natural external forces, such as other external mechanical operation interference activities, and belongs to Gaussian noise. Environmental noise is characterized by chaotic vibration and a wide spectrum, because the surrounding environment of the

occurrence and reception moment is uncertain, making the noise intensity unstable. The early fault shock response of the faulty bearing is relatively weak, and the influence of random noise is relatively strong, so the useful fault information is often submerged in the noise signal.

3. Basic Theory

3.1. Variational Mode Decomposition

VMD is a signal decomposition method based on variational Bayesian theory. It can iteratively search the optimal solution of a signal's variational model and perform multi-component decomposition according to the optimal solution to obtain a set of eigenmode functions orthogonal to each other and with different central frequencies and, at the same time, determine the central frequency and bandwidth of each modal function. Thus, the frequency domain division of the signal and the effective separation of each component can be realized.

The purpose of the VMD algorithm is to decompose a given rolling bearing signal $f(t)$ into several modal components $m_k(t), k = 1, 2, \cdots, K$, where K is a preset or estimated number of modes. The modal component is defined as the component modal function of amplitude and frequency modulation and is expressed by Formula (1).

$$m_k(t) = E(t)\cos[\psi_k(t)] \tag{1}$$

where $E(t)$ is the instantaneous amplitude and $\psi_k(t)$ is the phase.

Each modal function $m_k(t)$ will be approximately concentrated in the frequency domain around a central frequency ω_k; that is, this modal function has a small bandwidth. Moreover, the sum of these modal components should be able to reconstruct the original signal.

$$f(t) = \sum_{k=1}^{K} m_k(t) \tag{2}$$

The central frequency can be determined adaptively using a variational optimization framework, the core of which is achieved by frequency-domain energy-weighted averaging and iterative optimization.

$$\omega_k = \frac{\int_0^\infty \omega \left|\widehat{m}_k(\omega)\right|^2 d\omega}{\int_0^\infty \left|\widehat{m}_k(\omega)\right|^2 d\omega} \tag{3}$$

where $\widehat{m}_k(\omega)$ is the Fourier transform of $m_k(\omega)$.

The decomposition process of VMD is the process of solving the variational problem, and its algorithm mainly includes the construction of the variational problem and the solution of the variational problem. The variational problem is constructed as follows:

First, each modal function $m_k(t)$ is extended to the complex plane by Hilbert transformation, and its analytic signal is calculated by Formula (4).

$$f_k(t) = \left(\delta(t) + \frac{j}{\pi t}\right) * m_k(t) \tag{4}$$

where $\delta(t)$ is the unit pulse time function.

Second, the expression of transforming the modal function to the baseband can be expressed by Formula (5), multiplying Formula (2) with the pure exponential function of estimating the central frequency, that is, the bandwidth $F_k(t)$ is obtained by Formula (5).

$$F_k(t) = f_k(t)e^{-j\omega_k t} \tag{5}$$

Finally, in order to calculate each analytic signal, the Gaussian smoothness gradient norm is used as the bandwidth estimation, and each order mode is summed. The constrained variational model is established as follows:

$$\begin{cases} \min\limits_{\{\mu_k\},\{m_k\}} \left\{ \sum\limits_k \left\| \partial_t \left[(\delta(t) + \frac{j}{\pi t}) \cdot m_k(t) \right] e^{-j\omega_k t} \right\|_2^2 \right\} \\ s.t. \sum\limits_{k=1}^{k} m_k = f(t) \end{cases} \tag{6}$$

where ∂_t is the gradient operation.

The Lagrange multiplier $\lambda(t)$ and the quadratic penalty term α are introduced to transform Formula (6) into an unconstrained optimization problem. The extended Lagrange expression is as follows:

$$\begin{aligned} L(\{m_k\},\{\omega_k\},\lambda) = & \left\| m(t) - \sum_{k=1}^{K} m_k(t) \right\|_2^2 \\ & + \alpha \sum_{k=1}^{K} \left\| \partial_t \left[\left(\delta(t) + \frac{j}{\pi t} \right) \cdot m_k(t) \right] e^{-j\omega_k t} \right\|_2^2 \\ & + \left\langle \lambda(t), m(t) - \sum_{k=1}^{K} m_k(t) \right\rangle \end{aligned} \tag{7}$$

By alternating the direction multiplier method, m_k^{n+1}, central frequency ω_k^{n+1} and Lagrange multiplier λ_k^{n+1} are alternately updated in the frequency domain, and the "saddle point" expression of Lagrange expression is obtained as follows:

$$m_k^{n+1}(\omega) = \frac{m(\omega) - \sum\limits_{i \neq k} m_i(\omega) + \frac{\lambda(\omega)}{2}}{1 + 2\alpha(\omega - \omega_k)^2} \tag{8}$$

$$\omega_k^{n+1} = \frac{\int_0^\infty \omega |m_k(\omega)|^2 d\omega}{\int_0^\infty |m_k(\omega)|^2 d\omega} \tag{9}$$

$$\lambda^{n+1} = \lambda^n + \tau(m(\omega) - \sum_k m_k^{n+1}(\omega)) \tag{10}$$

When the mode satisfies the convergence condition in Formula (11), the VMD iteration stops.

$$\frac{\sum\limits_{k=1}^{K} \left\| m_k^{n+1}(\omega) - m_k^n(\omega) \right\|_2^2}{\left\| m_k^n(\omega) \right\|_2^2} < \sigma \tag{11}$$

where σ is the convergence threshold, and $\sigma > 0$.

According to the process of variational mode decomposition, when its core parameters are selected, it can decompose the rolling bearing signal into a set of modal functions with different frequencies and amplitudes, and the rolling bearing target signal and noise signal in the original signal will be decomposed into different modal components; thus, the modal component containing a noise signal can be eliminated. Meanwhile, it can be seen that the values of parameters α and K will affect the smoothness between the various modes in the calculation results. If the two parameters are not optimized, the calculation redundancy or calculation accuracy of the algorithm will be easily reduced during the iterative update calculation process, resulting in a poor algorithm denoising effect. So, it needs to be optimized.

3.2. Frost and Ice Algorithm

RIME [30] firstly covers parameter space by means of parallel population exploration to achieve global search, which can effectively avoid the mode aliasing caused by premature convergence. After the current optimal solution region is determined, a fine search is carried out to avoid the loss of signal details caused by over-decomposition or under-decomposition. The exploration strategy is gradually searched and developed, so as to achieve an efficient and high-precision search. The optimization idea is as follows:

First, each RIME particle is taken as the individual search of the algorithm, and the RIME population formed by all RIME particles is taken as the population of the algorithm. So, the RIME particle population is composed of n RIME factors S, each RIME factor is composed of d RIME particles, and the RIME particle cluster is initialized:

$$\begin{cases} R = \begin{bmatrix} D_1 \\ D_2 \\ \vdots \\ D_i \end{bmatrix} \\ D_i = \begin{bmatrix} r_{i1}, r_{i2}, \cdots, r_{ij} \end{bmatrix} \\ R = \begin{bmatrix} r_{11} & r_{12} & \cdots & r_{1j} \\ r_{21} & r_{22} & \cdots & r_{2j} \\ \vdots & \vdots & \ddots & \vdots \\ r_{i1} & r_{i2} & \cdots & r_{ij} \end{bmatrix} \end{cases} \tag{12}$$

Secondly, the RIME algorithm proposes a global search optimization method according to the movement characteristics of soft RIME particles in frost ice. By simulating the random growth process of each soft RIME particle, it realizes the rapid update of the position of the calculated RIME particles, so that the algorithm can quickly cover the entire search space in the early stage and avoid falling into the local optimal solution.

The soft RIME particle search process can be represented by Formula (13)

$$\begin{cases} R_{ij}^{new} = R_{best,j} + A_1 \cdot \cos\theta \cdot \gamma \cdot (h \cdot (U_{ij} - L_{ij}) + L_{ij}), A_2 < E_0 \\ E_0 = \sqrt{t/T} \\ \theta = \pi \cdot \frac{t}{10 \cdot T} \\ \gamma = 1 - \left(\frac{w \cdot t}{T}\right)/w \end{cases} \tag{13}$$

where $R_{best,j}$ is the position of the j-th optimal candidate solution; both A_1 and A_2 are random coefficients with the value range of $[-1, 1]$, which, together with $\cos\theta$, control the movement direction of soft RIME particles; t and T represent the number of iterations and the maximum iteration limit, respectively; γ represents the environmental factor, which is a step function that adjusts with the change in the number of iterations t to ensure the convergence of the algorithm; h is adhesion, which is used to control the distance between the two RIME particle centers; U_{ij} and L_{ij} are the upper and lower limits of the escape space, respectively, which limit the effective region of particle motion; E_0 is the adhesion coefficient, which affects the condensation probability of the particle and increases with the number of iterations.

At the same time, combining with the regular growth mechanism of hard RIME, a local search optimization algorithm for particle exchange is proposed, which can be expressed by Formula (14).

$$R_{ij}^{new} = R_{best,j}, A_3 < F_{normr}(D_i) \tag{14}$$

where A_3 is a random number in the interval $(-1, 1)$.

The RIME algorithm involves a positive greedy selection mechanism in the process of population renewal to improve the global search efficiency. The specific idea is as follows: the fitness values of individuals before and after the update are compared; if the fitness values of individuals after the update are better than those before the update, the two individuals and their solutions will be replaced as the optimal solution of this update, and then the global optimal solution will be obtained until the termination condition of the iterative update of the algorithm is met. The positive greedy selection mechanism enables the algorithm to continuously search for excellent particles in the iterative process, improves the quality of the global solution, and optimizes the iterative direction of the population, which can be expressed by Formula (15).

$$\begin{cases} \text{If } F(R_{i,j}^{new}) < F(R_{i,j}) \\ F(R_{i,j}) = F(R_{i,j}^{new}) \\ R_i = R_i^{new} \end{cases}, \begin{cases} \text{If } F(R_{i,j}^{new}) < F(R_{best,j}) \\ F(R_{best,j}) = F(R_{i,j}^{new}) \\ R_{best,j} = R_i^{new} \end{cases} \tag{15}$$

According to the new population location in the RIME algorithm, the core parameters of VMD can be obtained to improve the decomposition efficiency of the collected signal.

3.3. Fitness Function

The selection of a fitness function determines the final optimization decomposition effect, and this study selects the combination of power spectrum entropy and kurtosis value to establish the fitness function. According to the information entropy theory, the power spectrum entropy of a signal represents the sparse characteristics of the signal. When IMF has more noise and less characteristic information, the power spectrum entropy is larger, whereas the power spectrum entropy is smaller. The kurtosis value reflects the random variable distribution characteristic, which is sensitive to the rolling bearing signal. The specific construction method of the fitness function based on RIME-VMD is as follows:

The power spectrum of the IMF component after VMD decomposition is calculated, which is expressed by Formula (16).

$$e(f) = \frac{1}{2\pi L\prime}|F(\omega)|^2 \tag{16}$$

where $L\prime$ is the length of IMF component data and $F(\omega)$ is the discrete Fourier transform of the detected signal.

The power spectrum probability density function is obtained by normalizing the power spectrum, and the calculation function is as follows:

$$P_j = e_j / \sum_{j=1}^{N} e_j, j = 1, 2, \cdots, N \tag{17}$$

where e_j is the power spectrum value of the j-th IMF component and N is the number of discrete Fourier transform frequency components.

The power spectrum entropy is expressed by Formula (18).

$$IMF_{EE}(k) = -\sum_{j=1}^{N} P_j \log P_j \tag{18}$$

where $IMF_{EE}(k)$ is the envelope entropy of k modal signals.

In practical applications, if only the power spectrum entropy is used to establish the fitness function, the signal after decomposition is likely to be simple harmonics after optimization. This is because the power spectrum entropy only focuses on the spectrum

distribution, resulting in over-decomposition in signal decomposition and a serious loss of signal energy. For this reason, kurtosis is introduced to improve the signal over decomposition. Kurtosis is expressed by Formula (19).

$$IMF_Q(k) = \frac{E(f-\mu)^4}{\sigma_0^4} \tag{19}$$

where $IMF_Q(k)$ is the kurtosis value of k modal signals, μ is the mean of the signal, and σ_0 is the variance of the signal.

According to the Formulas (18) and (19), the fitness function is expressed by Formula (20).

$$fit = a \times IMF_{EE}(k) + b \times IMF_Q(k) \tag{20}$$

where a and b are the weight coefficients of the two parameters, respectively. When its value reaches the minimum, the VMD decomposition parameter with the best decomposition effect can be obtained.

4. Multi-Condition Rolling Bearing Fault Denoising Method Based on RIME-VMD

RIME-VMD uses the strong global search ability and efficient parameter update mechanism of the RIME algorithm to search the VMD decomposition level K and the penalty factor α, and it determines the optimal parameters. An algorithm flow chart is shown in Figure 2, and the detailed steps of the algorithm are as follows:

(1) The rolling bearing signal $f(t)$ is obtained and then put into the RIME initialization port, and the ranges of VMD key parameter combination (K, α) and relevant parameters in RIME are solved. These parameters include the maximum number of iterations, spatial dimensions, and so on.

(2) According to the obtained parameters, the signal is decomposed by using VMD, and K eigenmode functions (IMFs) from low frequency to high frequency are obtained. The fitness function value of each iteration is solved, and then the current minimum fitness function value and the corresponding local optimal solution are constantly updated and saved.

(3) According to Formula (14), the algorithm is updated and iterated continuously until the stopping condition is reached or the maximum number of iterations is met. Currently, the parameter combination corresponding to the lowest fitness function value is the optimal parameter combination.

(4) The VMD decomposition of the rolling bearing signal is performed using the optimal parameter combination to obtain the K components, and the envelope entropy and kurtosis values corresponding to each component are calculated. The components with large kurtosis and small envelope entropy are selected as the effective components with a high correlation degree and more characteristics of the target signal, and the effective components are decomposed again by VMD. After reconstruction, the optimal component IMF representing the characteristics of the target signal is generated, which is the effective fault frequency component signal of the rolling bearing signal extracted by RIME-VMD.

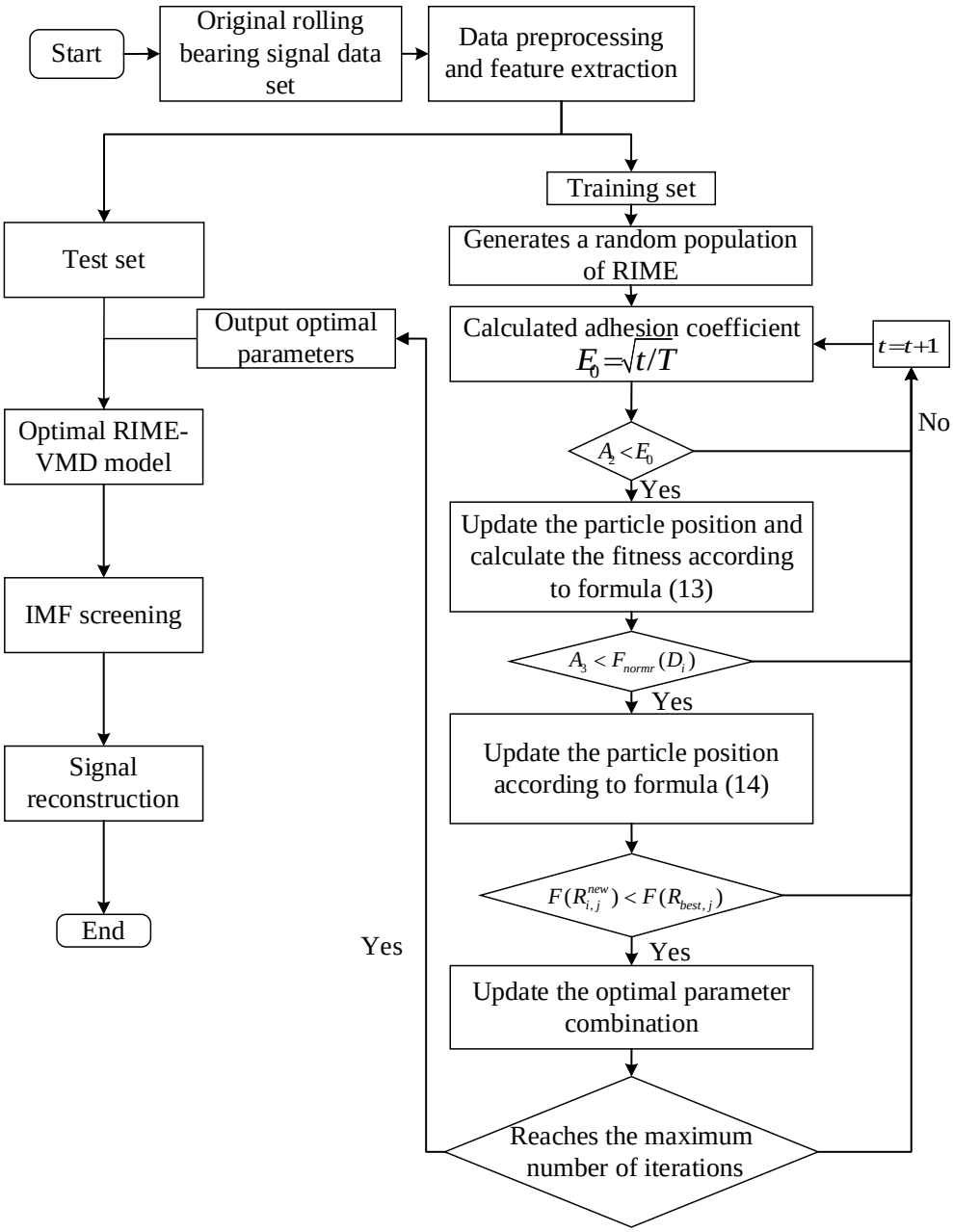


Figure 2. The algorithm flow chart.

The pseudo-code for RIME-VMD is shown in Algorithm 1.

Algorithm 1. Pseudo-Code of RIME-VMD

1: Initialize frost body population R
2: Obtain the current optimal parameter combination (K, α) and its optimal fitness functionss
3: While $t < T$
4: The adhesion coefficient is $E_0 = \sqrt{t/T}$
5: If $A_2 < E_0$
6: Update the parameter combination agent (K, α) location by soft RIME search policy
7: End if
8: If $A_3 < F_{normr}(D_i)$

Algorithm 1. *Cont.*

9: Cross-update between parameter combination agents (K, α) via the hard RIME mechanism
10: End if
11: If $F(R_i^{new}) < F(R_i)$
12: Select the optimal solution parameter combination (K, α) and its optimal fitness function fit and use the positive greedy selection mechanism to replace the sub-optimal solution
13: $t = t + 1$
14: End While

5. Experiment and Analysis

5.1. Experimental Dataset and Evaluation Index Settings

To verify the effectiveness of the proposed algorithm in the noise reduction processing of a rolling bearing signal under multiple working conditions, the XJTU-SY bearing dataset [31] is adopted as the verification dataset in this study. The XJTU-SY bearing dataset is based on the accelerated life test of rolling bearings carried out jointly by the School of Mechanical Engineering of Xi'an Jiaotong University and Zhejiang Changxing Shengyang Technology Co., Ltd., Shaoxing, China. The test bearing model is the LDK UER204 outer spherical rolling bearing. In the test, the sampling frequency was 25.6 kHz, the sampling interval was 1 min, and each sampling duration was 1.28 s. The rolling bearing signals are collected under three working conditions, and the speed and radial force of each working condition are also different.

To have an objective evaluation of the denoising performance of the algorithm, it should be evaluated from the aspects of the noise reduction performance of the algorithm, the difference between the reconstructed signal and the actual signal, and the transient impact detection of the fault signal, etc., so the commonly used evaluation indexes of signal denoising results are adopted. Five performance indicators, such as SNR (signal-to-noise ratio), RMSE (root mean square error), RC (reconstruction correlation), NCC (normalized correlation coefficient) and kurtosis, are used to quantitatively analyze the denoising effect of the signal. The larger the SNR, RC, NCC and kurtosis, the smaller the RMSE. The results indicate that the processed signal is more similar to the actual signal and the better noise reduction effect.

5.2. Experimental Environment and Parameter Configuration

The computer used in the experiment was configured with Windows 11 operating system, NVIDIA GeForce RTX4060 Laptop GPU, i5-11400H CPU, 16 GB memory. matlab2023a platform is used to run the RIME-VMD rolling bearing signal noise reduction algorithm designed in this study.

5.3. Ablation Experiment

To verify the effectiveness of the proposed algorithm in this study, a comparison experiment on the time–frequency domain reconstruction ablation of rolling bearing fault signals was conducted to compare the anti-noise reconstruction capabilities of the RIME-VMD method and VMD method in the case of noise.

In order to eliminate the errors caused by the different preset mode numbers of the two methods, RIME-VMD decomposition of the signal obtained the optimal total mode number of six and then set the total mode number of VMD to six. After the decomposition of the rolling bearing fault signal, it is necessary to screen the effective component and select the

effective component reconstruction with useful signal characteristics. The larger the SNR of the modal component, the more likely it is to be an effective component. The SNR of each mode obtained by the VMD algorithm calculated according to the principle of SNR is 7.31, 6.82, 5.44, 5.10, 5.31, and 4.87, and the SNR of each mode obtained by the RIME-VMD algorithm is as follows: 6.27, 8.74, 5.32, 5.46, 5.22, and 4.17. Therefore, VMD selects the first modal component as the effective component. RIME-VMD selects the second mode component as the effective component, and a comparison of the time-domain reconstructed signals of the two methods is shown in Figure 3. Among them, Figure 3a is the result of the time-domain reconstruction of the rolling bearing fault signal by using VMD, and Figure 3b is the result of the time-domain reconstruction of the rolling bearing fault signal by using RIME-VMD; the black line is the original rolling bearing fault signal, and the orange line is the reconstruction signal. The red area represents the rolling bearing signal at a certain moment, the blue area represents the noise signal.

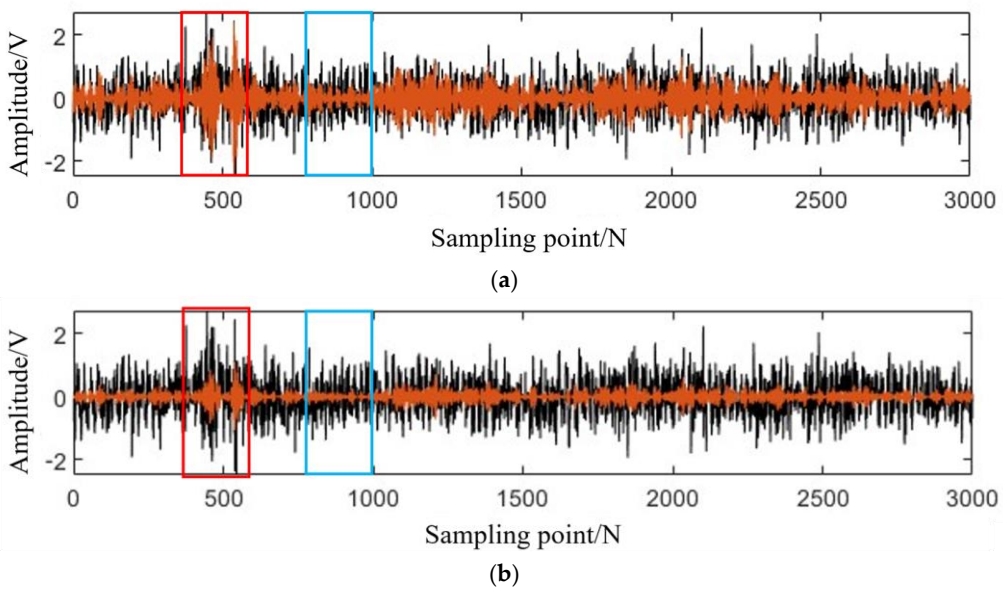


Figure 3. Comparison of time-domain reconstruction of rolling bearing fault signal. (**a**) the result of the time-domain reconstruction of the rolling bearing fault signal by using VMD; (**b**) the result of the time-domain reconstruction of the rolling bearing fault signal by using RIME-VMD.

As can be seen from Figure 3, both VMD and RIME-VMD can effectively remove part of the noise in rolling bearing fault signals. However, in the blue box in Figure 3a, it can be found that VMD cannot effectively remove low-frequency noise signals, thus reducing the noise reduction effect of the algorithm and increasing the difficulty of feature extraction and recognition of rolling bearing fault signals. Moreover, in the red box in Figure 3a, it can be seen that the noise reduction effect of high-frequency signals by using VMD is not ideal. The VMD algorithm cannot filter out all high-frequency interference signals, resulting in poor signal resolution, and it is more difficult to distinguish rolling bearing signals from the time domain. From the result of Figure 3b, it can be found that the RIME-VMD algorithm proposed in this study can effectively retain the fault signal and eliminate the interference signal.

The rolling bearing fault signal is reconstructed in the frequency domain, which is shown in Figure 4. Among them, Figure 4a is the result of the frequency-domain reconstruction of the rolling bearing fault signal by using VMD; Figure 4b is the result of the frequency-domain reconstruction of the rolling bearing fault signal by using RIME-VMD. The red box represents the part where the results obtained by the two methods differ.

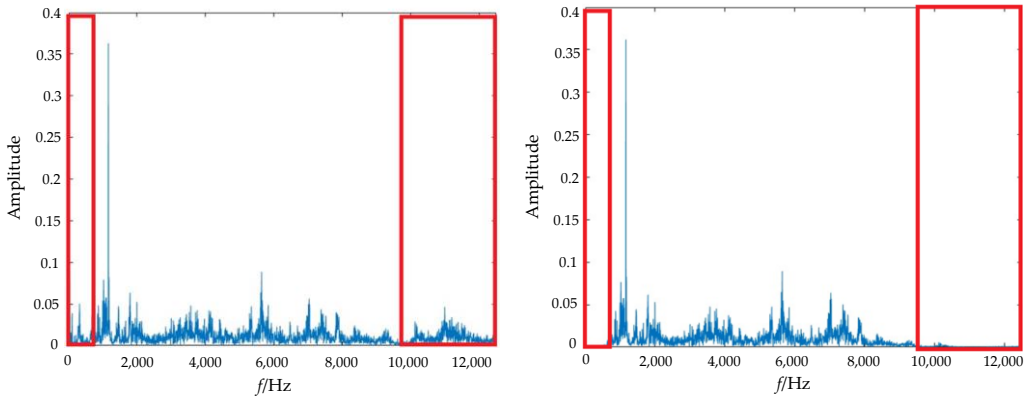


Figure 4. Comparison of frequency-domain reconstruction of rolling bearing fault signal. (**a**) the result of the frequency-domain reconstruction of the rolling bearing fault signal by using VMD; (**b**) the result of the frequency-domain reconstruction of the rolling bearing fault signal by using RIME-VMD.

As can be seen from Figure 4a, VMD cannot effectively remove low-frequency noise and high-frequency noise in the red box, resulting in a lot of noise in the rolling bearing fault signal, which makes it more difficult to extract effective fault characteristics in the future. As can be seen from Figure 4b, the RIME-VMD algorithm in this study can effectively solve this problem, not only retaining useful frequencies in the rolling bearing fault signal but also filtering out low-frequency and high-frequency noise. The results show that this method can achieve a better noise reduction in the rolling bearing fault signal.

The reconstruction accuracy of the RIME-VMD and VMD methods was compared from the perspective of quantization and analyzed using RMSE, SNR and RC. The result is shown in Table 1.

Table 1. Performance comparison of signal decomposition and reconstruction methods between VMD and RIME-VMD.

Signal Decomposition and Reconstruction Method	RMSE	RC	SNR/dB	NCC	Kurtosis
VMD	0.482	0.9213	11.56	0.813	4.978
RIME-VMD	0.047	0.9849	13.32	0.984	5.682

In terms of correlation, RIME-VMD in time-domain reconstruction and frequency-domain reconstruction reached above 0.9849, which was highly coincident with the original analysis signal, while the time-domain reconstruction correlation and frequency-domain reconstruction correlation of VMD was 0.9213, and the RMSE and SNR of RIME-VMD are better than that of VMD, which means it can obtain reconstructed signals with less noise. The reconstruction correlation of RIME-VMD was better than that of VMD.

5.4. Sensitivity Analysis of RIME Parameters Affecting the Denoising Performance

In order to verify the impact of RIME parameters on the noise reduction performance of VMD, a comparative test was designed by using different particle populations and numbers of iterations, and the result is shown in Table 2.

Table 2. The result of RIME parameters affecting the denoising performance.

NO.	Particle Population/N	Number of Iterations/T	RMSE	RC	SNR/dB	NCC	Kurtosis	Computation Time/s
1	10	30	0.473	0.918	8.31	0.773	4.978	61.34
2	30	50	0.154	0.982	12.51	0.954	5.682	150.68
3	50	100	0.132	0.985	12.17	0.912	5.311	319.91

As shown in Table 2, three groups of different RIME parameters are designed for comparison. It can be seen that the number of designed particles in the first group is 10 and the number of iterations is 30. Although the calculation time is short, the SNR and RC of the reconstructed signal for noise reduction are the lowest, RMSE is the highest, and the noise reduction performance is the worst. The third group sets the largest number of particles and number of iterations. The large-scale iterative optimization effectively guarantees the SNR, RC, NCC and kurtosis of the reconstructed signal; the RMSE becomes low but also greatly increases the calculation time and poor real-time performance. The parameter settings of the second group are reasonable, which not only ensures the index of the noise reduction and reconstruction signal but also reduces the calculation time, so the second group is selected for subsequent optimization.

5.5. Comparative Experimental Analysis

To verify the superiority of the experiment in this study, different swarm intelligent optimization algorithms are used to compare the optimization effects of VMD parameter selection. In order to verify the superiority of RIME in VMD parameter optimization, in this section, four classical optimization algorithms, namely RIME, SSA [32], PSO [33] and HHO [34], are mainly compared in terms of their convergence speed and optimal fitness value in the VMD parameter optimization process.

As shown in Figure 5, the PSO algorithm reaches the minimum entropy at the seventh iteration, and its convergence speed is slow; the SSA algorithm and HHO algorithm both reach the minimum entropy at the fifth iteration, but the fitness function is slightly larger than that obtained by RIME, resulting in low convergence accuracy; and the RIME algorithm has the most significant advantage over the other three algorithms, namely fast convergence speed. At the fifth iteration, the entropy reaches the minimum, and the fitness is the smallest. The results show that the RIME algorithm is more ideal than other intelligent optimization algorithms in optimizing the VMD parameter selection process.

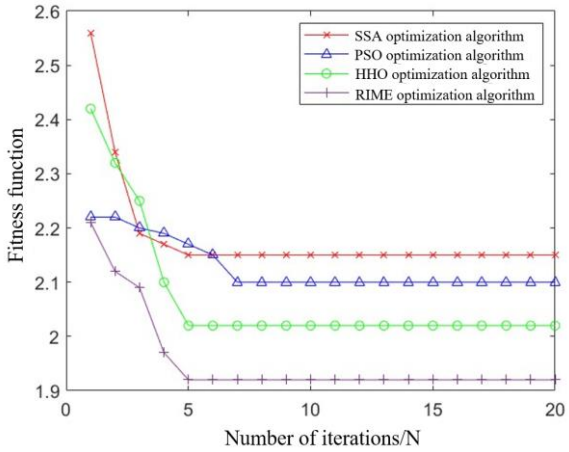


Figure 5. Comparison of iteration results of different optimization algorithms.

To verify the adaptability of the proposed algorithm under various working conditions, the bearing data under two different working conditions in the XJTU-SY bearing dataset are compared with the three methods. The fitness functions of different optimization algorithms under working condition 1 are shown in Figure 6, and the performance comparison results under working condition 1 are shown in Table 3. Among them, working condition 1 is that the rotational speed is 2100 r/min and radial force is 12 KN; the fitness functions of different optimization algorithms under working condition 2 are shown in Figure 7, and the performance comparison results under working condition 2 are shown in Table 4. Among them, working condition 2 is that the rotational speed is 2400 r/min and radial force is 10 KN.

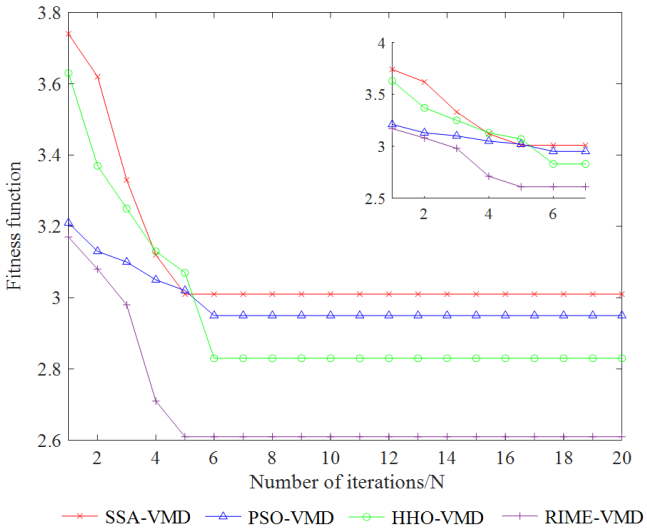


Figure 6. The fitness functions of different optimization algorithms under working condition 1.

Table 3. Performance comparison of different signal decomposition and reconstruction methods under working condition 1.

Working Condition	Signal Decomposition and Reconstruction Method	RMSE	RC	SNR	NCC	Kurtosis
Rotational speed: 2100/(r/min) Radial force: 12/KN	SSA-VMD	0.585	0.881	11.56	0.784	5.81
	PSO-VMD	0.426	0.935	10.77	0.792	5.53
	HHO-VMD	0.107	0.908	9.20	0.761	5.01
	RIME-VMD	0.067	0.991	13.29	0.845	5.92

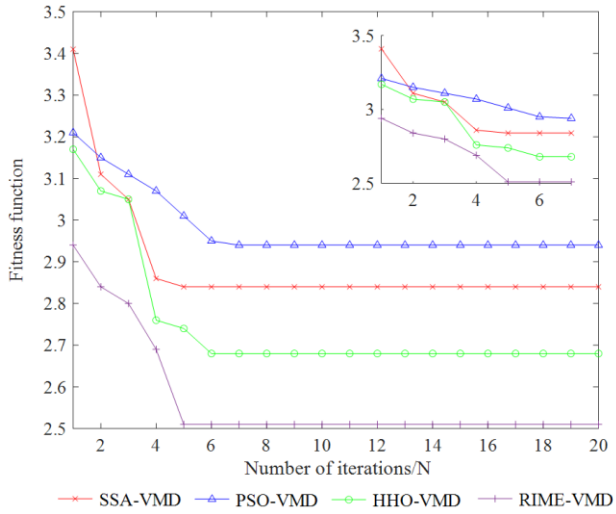


Figure 7. The fitness functions of different optimization algorithms under working condition 2.

Table 4. Performance comparison of different signal decomposition and reconstruction methods under working condition 2.

Working Condition	Signal Decomposition and Reconstruction Method	RMSE	RC	SNR	NCC	Kurtosis
Rotational speed: 2100/(r/min) Radial force: 12/KN	SSA-VMD	0.677	0.923	9.56	0.657	5.32
	PSO-VMD	0.421	0.918	9.98	0.778	5.11
	HHO-VMD	0.302	0.852	8.78	0.721	5.54
	RIME-VMD	0.071	0.984	12.95	0.821	5.87

It can be seen from Figures 6 and 7 that, although the SSA algorithm can achieve rapid convergence, the initial value of the fitness obtained by the algorithm is relatively large, indicating that the algorithm has a poor ability to obtain the initial solution. The PSO algorithm can obtain a better initial solution, but the optimization result is poor. Although the HHO algorithm can obtain a lower fitness function, it requires more iterations to obtain the optimal solution, takes a longer time, and its ability to obtain solutions is unstable when facing bearing fault signals under different working conditions. However, in the fifth iteration of the RIME algorithm, the global fitness reaches the minimum and a stable solution can be obtained. The results show that, in the process of optimizing the parameter selection of VMD, the RIME algorithm is more ideal than other intelligent optimization algorithms.

According to the results in Tables 3 and 4, the reconstruction results of the SSA optimization algorithm are unstable when the working conditions change, and it can be seen that the change in RMSE, RC and NCC is larger. The reconstruction result of the PSO algorithm is relatively stable, the RC is larger, but the RMSE of the reconstructed signal is also larger. The RMSE of the HHO optimization algorithm is small, and the SNR and NCC are small, which means the signal is easily submerged in the noise. However, the performance of the proposed algorithm is relatively stable under different working conditions, and the performance of the signal evaluation functions, such as RMSE, SNR, RC, NCC and kurtosis, is better, which proves the stability of the proposed algorithm's noise reduction ability under different working conditions.

6. Conclusions

Aiming at the strong noise interference problem of a rolling bearing fault signal under different working conditions, this study proposes a multi-condition rolling bearing fault denoising method based on RIME-VMD. In order to realize the adaptive selection of the VMD mode number and quadratic penalty factor, the RIME algorithm was adopted, and the VMD parameter self-optimizing search ability was improved by constructing a fitness function. Based on the optimal mode number and quadratic penalty factor, the VMD decomposition of a rolling bearing fault signal was performed, and the correlation coefficient screening method was used to screen the IMF component; signal reconstruction was carried out to achieve signal noise reduction. Through the experiment, the proposed method and VMD method are compared and analyzed, and the results show that the proposed method has a better noise reduction effect in rolling bearing fault signal noise reduction compared to the five evaluation indexes. Combined with different optimization algorithms, the noise reduction effect of the rolling bearing fault signal under multiple working conditions is compared and tested to verify the stability of the noise reduction algorithm in this study. In order to improve the accuracy of rolling bearing fault diagnosis, the future research direction should not only consider the noise reduction algorithm with good noise reduction performance but also introduce multi-source sensors to collect the

signals of the equipment in the running state. At the same time, multi-source signals are fused through deep learning to provide a means for the next step in fault diagnosis.

Author Contributions: Conceptualization and methodology, software and validation, writing—original draft, X.Z.; methodology, software and validation, writing—original draft, X.L.; methodology, software and validation, writing—original draft, H.L. All authors have read and agreed to the published version of the manuscript.

Funding: This work was supported by Shaanxi Provincial Science and Technology Department (Grant No. 2023-YBGY-342).

Data Availability Statement: The data that support the findings of this study are available from the corresponding author upon reasonable request.

Conflicts of Interest: The authors declare no conflicts of interest.

References

1. Wang, J.; Li, H.; Zhang, W.; Chen, Y. Adaptive modal total variational mode decomposition method and its performance evaluation. *J. Vib. Shock* **2023**, *42*, 251–262.
2. Phan, V.; Vo, C.; Dao, H.; Ahn, K. Robust fault-tolerant control of an electro-hydraulic actuator with a novel nonlinear unknown input observer. *IEEE Access* **2021**, *9*, 30750–30760. [CrossRef]
3. Burda, E.; Zusman, G.; Naumenko, A. An overview of vibration analysis techniques for the fault diagnostics of rolling bearings in machinery. *Shock Vib.* **2022**, *2022*, 6136231. [CrossRef]
4. Liu, J.; Shao, Y. Overview of dynamic modelling and analysis of rolling element bearings with localized and distributed faults. *Nonlinear Dyn.* **2018**, *93*, 1765–1798. [CrossRef]
5. Xie, C.; Wang, X.; Xiao, F.; Peng, C.; Mei, Y.; Liu, P. Review of bearing fault modes and fault diagnosis methods. *Comput. Meas. Control* **2024**, 1–11.
6. Zhang, Y.; Zhang, T.; Ge, P.; Wang, C.; Wang, Y. Review on intelligent fault diagnosis of motor bearings. *Mech. Electr. Eng. Technol.* **2024**, *53*, 1–6.
7. Liu, Z.; Yu, H.; Miao, X. RMCW: An improved residual network with multi-channel weighting for machinery fault diagnosis. *IEEE Access* **2023**, *11*, 124472–124483. [CrossRef]
8. Smith, W.; Randall, R. Rolling element bearing diagnostics using the case western reserve university data: A benchmark study. *Mech. Syst. Signal Process.* **2015**, *64–65*, 100–131.
9. Ding, J.; Huang, L.; Li, X. GMPSO-VMD Algorithm and its application to rolling bearing fault feature extraction. *Sensors* **2020**, *20*, 1946. [CrossRef]
10. Xiao, F.; Yang, D.; Wang, Y. VMD-based denoising methods for surface electromyography signals. *J. Neural Eng.* **2019**, *16*, 056017. [CrossRef]
11. Bian, J.; Jing, L.; Liu, Y. Application of entropy theory in bearing fault diagnosis. *J. Dalian Polytech. Univ.* **2024**, *43*, 300–306.
12. Gu, J.; Peng, Y. An improved complementary ensemble empirical mode decomposition method and its application in rolling bearing fault diagnosis. *Digit. Signal Process.* **2021**, *113*, 103050. [CrossRef]
13. Zhou, J.; Xiao, M.; Ji, G. Rolling Bearing Fault Diagnosis Based on WGWOA-VMD-SVM. *Sensors* **2022**, *22*, 6281. [CrossRef] [PubMed]
14. Chen, S.; Peng, Z.; Zhou, P. Review of Signal Decomposition Theory and Its Applications in Machine Fault Diagnosis. *J. Mech. Eng.* **2020**, *56*, 91–107.
15. Fan, H.; Xu, H.; Fan, W.; Chen, B.; Li, Q.; Zhang, T.; Cao, X.; Zhang, X. Cloud–edge collaborative intelligent fault diagnosis of rotor-bearing system: Methodology and experiment. *IEEE Sens. J.* **2025**, *25*, 5044–5059. [CrossRef]
16. Li, H.; Zhang, X. An equivalent target plate damage probability calculation mathematics model and damage evaluation method. *Def. Technol.* **2024**, *41*, 82–103. [CrossRef]
17. Sun, M.; Li, Z.; Li, Z.; Li, Q.; Liu, Y.; Wang, J. A noise attenuation method for weak seismic signals based on compressed sensing and CEEMD. *IEEE Access* **2020**, *8*, 71951–71964. [CrossRef]
18. Liu, F.; Gao, J.; Liu, H. The feature extraction and diagnosis of rolling bearing based on CEEMD and LDWPSO-PNN. *IEEE Access* **2020**, *8*, 19810–19819. [CrossRef]
19. Li, H.; Zhang, X.; Kang, W. A testing and data processing method of projectile explosion position based on three UAVs' visual spatial constrain mechanism. *Expert Syst. Appl.* **2025**, *265*, 125984. [CrossRef]
20. Li, H.; Zhang, X.; Gao, J. A projectile signal recognize algorithm using variational mode decomposition and wavelet mode maximum fusion in sky screen sensor and its application. *IEEE Sens. J.* **2024**, *24*, 40648–40658. [CrossRef]

21. Zhao, Y.; Ma, Y.; Chen, J. Noise reduction based on a CEEMD-WPT crack acoustic emission datase. *Appl. Sci.* **2023**, *13*, 10274. [CrossRef]
22. Li, H.; Liu, T.; Chen, Q. An optimized VMD method and its applications in bearing fault diagnosis. *Measurement* **2020**, *166*, 108185. [CrossRef]
23. Cui, H.; Guan, Y.; Chen, H. Rolling element fault diagnosis based on VMD and sensitivity MCKD. *IEEE Access* **2021**, *9*, 120297–120308. [CrossRef]
24. Quan, Y.; Yu, M.; Wang, W.; Wei, L. Short-term wind speed prediction based on fractal optimization of VMD-GA-BP. *Acta Energiae Solaris Sin.* **2023**, *44*, 436–446.
25. Jiang, L.; Lu, X.; Wang, J.; Yu, M. Feature parameters extraction method of gear based on PSO-VMD. *Manuf. Technol. Mach. Tool* **2017**, *11*, 65–71.
26. Chen, W.; Li, J.; Zhang, W. Rolling bearing fault diagnosis based on VMD hybrid domain feature and SSA-SVM. *Mach. Tool Hydraul.* **2022**, *50*, 159–164.
27. Zhong, X.; Zhao, Y.; Hu, J. Application of total variation denoising based on particle swarm optimization in bearing fault diagnosis. *Machinery* **2020**, *47*, 1–5+21.
28. Chen, C.; Zhou, L.; Yang, L. Axle box bearing fault diagnosis based on average autocorrelation and optimized VMD. *J. Vib. Meas. Diagn.* **2023**, *43*, 231–239+405.
29. Qin, Y.; Li, G.; Qi, J.; Wang, J. Fault diagnosis of transverse damper for high-speed trains based on RIME-VMD. *J. Railw. Sci. Eng.* **2024**, *46*, 761.
30. Li, H.; Li, M.; Ma, Y.; Zheng, Y.; Li, S. A variational mode decomposition projectile signal processing algorithm of infrared sky screen velocity measurement system and detection mathematical model of detection screen. *Optik* **2023**, *287*, 171077. [CrossRef]
31. Lei, Y.; Han, T.; Wang, B.; Li, N.; Yan, T.; Yang, J. XJTU-SY Rolling element bearing accelerated life test datasets: A tutorial. *J. Mech. Eng.* **2019**, *55*, 1–6.
32. Wang, M.; Wang, W.; Zhang, Y. An integrated method based on sparrow search algorithm improved variational mode decomposition and support vector machine for fault diagnosis of rolling bearing. *J. Vib. Eng. Technol.* **2022**, *10*, 2893–2904. [CrossRef]
33. Mao, M.; Chang, J.; Wang, Z. Research on VMD-based adaptive TDLAS signal denoising method. *Photonics* **2023**, *10*, 674. [CrossRef]
34. Zhang, B.; Su, Y.; Jiang, Y. Bearing fault diagnosis based on improved variational mode decomposition and optimized stacked denoising autoencoder. *Comput. Integr. Manuf. Syst.* **2024**, *30*, 1408–1421.

Disclaimer/Publisher's Note: The statements, opinions and data contained in all publications are solely those of the individual author(s) and contributor(s) and not of MDPI and/or the editor(s). MDPI and/or the editor(s) disclaim responsibility for any injury to people or property resulting from any ideas, methods, instructions or products referred to in the content.